


Article

Earlier Detection of Alzheimer's Disease Based on a Novel Biomarker *cis* P-tau by a Label-Free Electrochemical Immunosensor

Ayoub Shiravandi ¹, Farzaneh Yari ², Nahid Tofigh ³, Mohammad Kazemi Ashtiani ¹, Koorosh Shahpasand ⁴, Mohammad-Hossein Ghanian ^{1,*} , Faezeh Shekari ^{5,*} and Farnoush Faridbod ²

¹ Department of Cell Engineering, Cell Science Research Center, Royan Institute for Stem Cell Biology and Technology, Academic Center for Education, Culture and Research (ACECR), Tehran 1665659911, Iran

² Center of Excellence in Electrochemistry, School of Chemistry, College of Science, University of Tehran, Tehran P.O. Box 14155-6455, Iran

³ Laboratory of Neuro-Organic Chemistry, Institute of Biochemistry and Biophysics (IBB), University of Tehran, Tehran 1417935840, Iran

⁴ Department of Stem Cells and Developmental Biology, Cell Science Research Center, Royan Institute for Stem Cell Biology and Technology, Academic Center for Education, Culture and Research (ACECR), Tehran 1665659911, Iran

⁵ Advanced Therapy Medicinal Product Technology Development Center, Royan Institute for Stem Cell Biology and Technology, Academic Center for Education, Culture and Research (ACECR), Tehran 1665659911, Iran

* Correspondence: ghanian@royaninstitute.org (M.-H.G.); faezhshekari@royaninstitute.org (F.S.)

Abstract: Early detection of *cis* phosphorylated tau (*cis* P-tau) may help as an effective treatment to control the progression of Alzheimer's disease (AD). Recently, we introduced for the first time a monoclonal antibody (mAb) with high affinity against *cis* P-tau. In this study, the *cis* P-tau mAb was utilized to develop a label-free immunosensor. The antibody was immobilized onto a gold electrode and the electrochemical responses to the analyte were acquired by electrochemical impedance spectroscopy (EIS), cyclic voltammetry (CV), and differential pulse voltammetry (DPV). The immunosensor was capable of selective detection of *cis* P-tau among non-specific targets like *trans* P-tau and major plasma proteins. A wide concentration range (10×10^{-14} M– 3.0×10^{-9} M) of *cis* P-tau was measured in PBS and human serum matrices with a limit of detection of 0.02 and 0.05 pM, respectively. Clinical applicability of the immunosensor was suggested by its long-term storage stability and successful detection of *cis* P-tau in real samples of cerebrospinal fluid (CSF) and blood serum collected from human patients at different stages of AD. These results suggest that this simple immunosensor may find great application in clinical settings for early detection of AD which is an unmet urgent need in today's healthcare services.

Keywords: Alzheimer's disease; early detection; antibody; *cis* P-tau; human serum; electrochemical biosensor



Citation: Shiravandi, A.; Yari, F.; Tofigh, N.; Kazemi Ashtiani, M.; Shahpasand, K.; Ghanian, M.-H.; Shekari, F.; Faridbod, F. Earlier Detection of Alzheimer's Disease Based on a Novel Biomarker *cis* P-tau by a Label-Free Electrochemical Immunosensor. *Biosensors* **2022**, *12*, 879. <https://doi.org/10.3390/bios12100879>

Received: 13 September 2022

Accepted: 7 October 2022

Published: 17 October 2022

Publisher's Note: MDPI stays neutral with regard to jurisdictional claims in published maps and institutional affiliations.



Copyright: © 2022 by the authors. Licensee MDPI, Basel, Switzerland. This article is an open access article distributed under the terms and conditions of the Creative Commons Attribution (CC BY) license (<https://creativecommons.org/licenses/by/4.0/>).

1. Introduction

Alzheimer's disease (AD) is a chronic, devastating dysfunction of neurons in the brain characterized by progressive memory impairment, noticeable personality changes, cognitive impairment, dementia, and eventual death [1]. AD represents one of the biggest medical challenges over the past five decades [1–4]. According to the World Health Organization (WHO), more than 50 million people suffer from dementia and this number is expected to exceed 152 million by the year 2050 [5,6]. One of the biggest challenges in control of AD is the early diagnosis of disease which is crucial for effectiveness of the drugs and subsequently less nerve damage [4,7–10]. By early detection of AD in the first stages of the disease, the routine treatments can be more effective to prevent disease progression and reduce the mortality and healthcare costs [9,10].

AD is considered a continuum of gradual brain changes progressing over about 25 years before the first symptoms appear [11]. In the early stages of AD, with the low concentration of biomarkers, the AD is a mild cognitive impairment (MCI), but over time and as the amount of disease-causing agents increases, AD appears with all its associated symptoms [12]. Therefore, AD has the potential to be diagnosed before the dementia stage. The advanced tools of AD diagnosis are still incapable of early detection, mainly due to the lack of a biorecognition element for the earlier biomarkers of AD. Currently, the most well-known biomarkers that are agreed upon are the tau proteins and amyloid- β peptides. These biomarkers are identified in cerebrospinal fluid (CSF) samples, which are commonly used for AD diagnosis in clinical practice [10,13]. In this regard, a variety of biosensors have been developed in the literature for more accurate and rapid diagnosis of AD based on these biomarkers [14–30]. However, none of these biomarkers is the exclusive early driver of the disease which can be meaningfully detected at early stages of the disease. Hence, there is an unmet need for a biosensor based on an early stage biomarker of AD.

Tau is a microtubule-related protein that contributes to stabilizing microtubules in neural cells [22]. The abnormal phosphorylation process of tau proteins is an essential characteristic of tau pathology in AD [31] because the hyperphosphorylated tau (P-tau) proteins aggregate in the form of paired helical filaments which form intracellular neurofibrillary tangles (NFTs) in the dendritic spines of neurons [32]. By increasing and deposition of NFTs, the normal function of nerve cells is disrupted which eventually leads to cell death [33,34]. The P-tau protein exists in two conformations, *trans* and *cis*, of which the latter has been shown to be extremely neurotoxic and more prone to accumulation [35–38]. Clinical data shows that in the early stages of AD, an increase in the concentration of the *cis*, but not *trans*, isoform of P-tau appears in the brains of humans with MCI [39–42]. In addition, the concentration of *cis* P-tau increases more severely than other pathogenic species of tau tangles in AD [38,43–45]. This robust *cis* P-tau pathology (cistauosis) has been also seen after traumatic brain injury in humans and mice which is the best-known environmental risk factor for AD. These data show that the cistauosis appears long before other tauopathy factors and can be considered as a precursor of tauopathy and a specific signal to predict AD at the earlier stages [36,39,41,46–49]. However, no biosensor has been developed for AD detection based on cistauosis. Particularly, *cis* pT231-tau is a central mediator and an early driver of neurodegeneration upon tauopathy process. Moreover, it has a prion nature and spreads in the CSF as well as blood. Thus, we herein employed a monoclonal antibody against the pathogenic P-tau species to detect and even predict neurodegeneration through a non-invasive procedure using blood samples.

The cut-off value of P-tau in CSF is considered in the range of 10 to 20 pM [50]; however, the serum level of P-tau is expected much lower (~20 times) because P-tau levels in brain is amplified by spilling of intracellular tau from dying neurons in the central nervous system which are in direct contact with CSF [51]. As a result, the concentration of P-tau in CSF is proportional to the amount of released protein from the brain neurons, while the P-tau content in serum is determined by the amount of protein released from CSF into serum, which is limited by the relatively large size of P-tau that limits its permeability through the blood–brain barrier [52]. Due to the extremely low levels of P-tau in serum, current assay methods cannot be used to detect P-tau in blood samples [53]. In addition, the serum concentration of *cis* P-tau is further lower than that of the total P-tau due to co-existence of the two conformations (*cis* and *trans*) of P-tau in human serum [35,36], and hence a highly sensitive measurement is required to detect *cis* P-tau in serum [54–56].

Recently, we developed a monoclonal antibody (mAb) against the *cis* isoform of P-tau protein, which showed selectivity to block this driver of AD and delayed the progression of AD in mice [39]. Thereafter, we established a *cis* P-tau mAb with high affinity against the human samples [53]. This proprietary human *cis* P-tau mAb has been exploited in this work to develop an immunosensor for earlier detection of AD based on cistauosis. To establish an easy-to-use biosensor platform, the antibody was immobilized on the surface gold electrodes, and the signal changes upon analyte addition were acquired by conventional

electrochemical analyses. This label-free detection mechanism allows for easy, fast, and cost-effective analysis without the need for labeling the analyte with the signal tags (e.g., enzymes and metal nanoparticles).

Our result shows applicability of this simple biosensor in clinical settings for early detection of AD.

2. Materials and Methods

2.1. Materials

Briefly, 3-Mercaptopropionic acid (MPA, 99%), 11-Mercaptoundecanoic acid (MUA, 98%), N-(3-dimethyl amino propyl)-N' ethyl carbodiimide hydrochloride (EDC), N-hydroxysuccinimide (NHS), bovine serum albumin (BSA), potassium ferricyanide ($K_3Fe(CN)_6$), potassium ferro cyanide ($K_4Fe(CN)_6$), sodium hydroxide (NaOH), phosphate buffered saline (PBS: 10 mM Na_2HPO_4 , 10 mM KH_2PO_4 , 150 mM NaCl, pH 7.5), potassium chloride (KCl), ethanol 99%, HRP-conjugated goat anti-mouse IgG antibody, beta-2-microglobulin, immunoglobulin g ($\geq 95\%$), hemoglobin, 3,3',5,5'-tetramethylbenzidine (TMB), and sulfuric acid (H_2SO_4 , 99%) were purchased from Sigma-Aldrich. Human albumin (20%) was purchased from Biotest Pharma GmbH (Germany). Alumina powder (5.0, 0.30, and 0.1 μm) was purchased from Metsuco (Houston, USA) and Sigma-Aldrich (Bengaluru, Karnataka, India). Yellow lumbar puncture needle (20-gauge) was purchased from Millipore (Frankfurter, Germany). Screen-printed gold electrodes (SPGE) (Aux.: Pt; Ref.: Ag)/Ink AT and gold disk electrodes (GDE) were purchased from Metrohm (Herisau, Switzerland) and Azar Electrode (Urmia, Iran), respectively. Ultrapure deionized water (Milli-Q, 18.2 $M\Omega$ cm) was obtained from the Milli-Q system and used in the experiments and washing.

2.2. Electrode Preparation

For the purpose of removing and cleaning any impure materials from the GDE surface, first, the bare electrodes were polished with alumina powders (5.0, 0.30, and 0.1 μm) for 5 min with each of the sizes, subsequently immersed in piranha solution (1:3, 30% H_2O_2 and concentrated 98% H_2SO_4) for 5 min, and then rinsed with deionized water. To achieve a maximum cleaning, the GDE was cleaned by electrochemical method in 0.5 M NaOH solution via cyclic voltammetry (CV) at 0.1 V/s scan rate and in the -0.3 to 0.8 V potential range. Then electrodes were immersed into 0.5 M H_2SO_4 and CV conducted at 0.1 V/s scan rate and in the -0.3 to 0.8 V potential range. After the processes, the GDE was washed with deionized water and dried.

2.3. Fabrication of Immunosensor

Cis P-tau mAb, the same clone as #113 from Creativebiolabs, was produced with $\sim 99\%$ purity in the lab according to the procedure of our previous publications [57]. The immunosensor was fabricated by covalent immobilization of the antibody on the surface of the gold electrode (Figure 1). Two thioacid cross-linkers (MPA and MUA) were used to establish attachment sites on the gold for antibody immobilization. A mixture of MUA/MPA (70/30) in ethanol (10 mM) was dropped on the gold surface and dried for 8 h at room temperature (RT). The linker-modified electrode was washed by ethanol to remove all non-bonded molecules. Then, a mixture of EDC (20 mM)/NHS (5 mM) in 0.1 M PBS (pH = 5.5–6) was dropped onto the surface at RT and left to dry. Next, a PBS solution of *cis* P-tau mAb (10 $\mu g/mL$, pH 7.5) was dropped onto surface and kept overnight at 4 °C to dry and then rinsed with PBS solution. In the last stage, to block non-specific adsorption, a PBS solution of BSA (1% *w/v*) was dropped onto the electrode surface, kept for 1 h, and rinsed with PBS. The immunosensors based on SPGE were fabricated via a similar protocol, without need for the initial electrode cleaning. The fabricated immunosensors were stored at 4 °C until use.

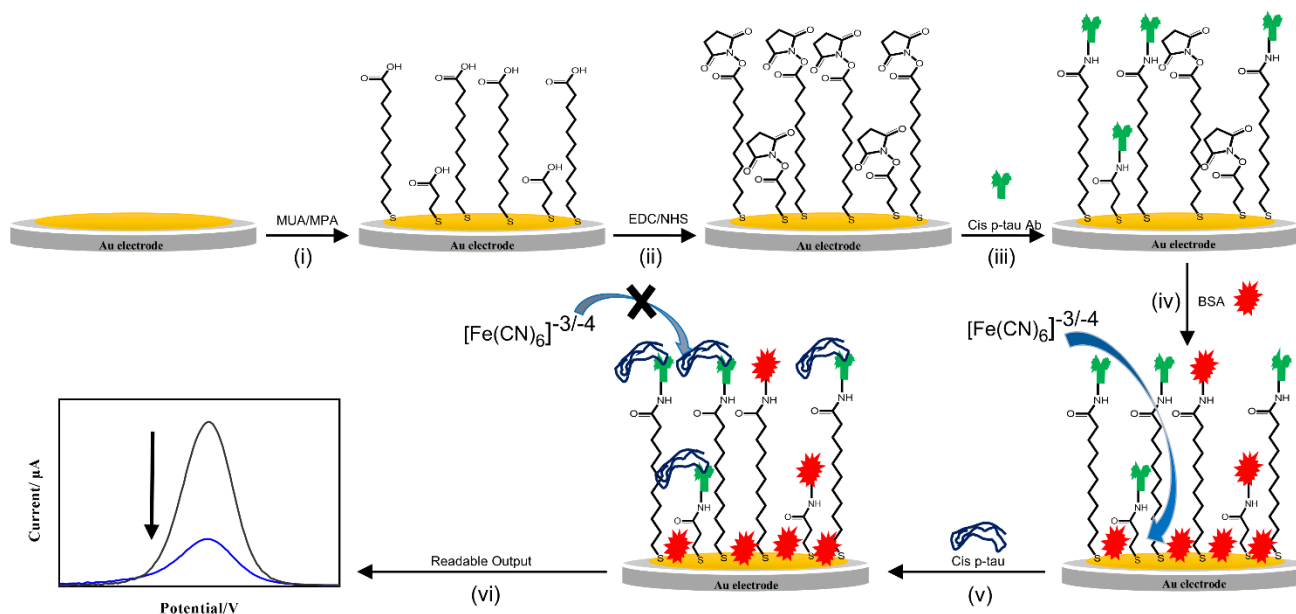


Figure 1. Schematic illustration of immunosensor fabrication and mechanism of performance. (i) Surface modification of gold electrode with the thiol linkers (11-Mercaptoundecanoic acid; MUA and 3-Mercaptopropionic acid; MPA), (ii) activation of the linkers with EDC/NHS, (iii) immobilization of the *cis* P-tau antibody, (iv) blocking of non-specific sites by BSA, (v) addition of the *cis* P-tau and connecting it to the antibody and increasing the resistance of the sensor surface, and (vi) production of a readable signal.

2.4. Morphological Characterization of Immunosensor Surface

In each step of the immunosensor assembly, the surface morphologies of the electrodes were analyzed over a $10 \times 10 \mu\text{m}$ area by atomic force microscopy (AFM; VEECO CP II, Veeco Instruments Inc., New York, NY, USA). The imaging process was operated in contact mode, and scanned at a rate of 1.0 Hz. To show the capability for *cis* P-tau interaction with the immobilized antibody, the modified electrode was subjected to incubation with the *cis* P-tau solution in PBS (1.0×10^{-12} M) for 30 min at RT, followed by washing with 5 mL of PBS before imaging.

2.5. Electrochemical Characterization of Immunosensor

Electrochemical impedance spectroscopy (EIS) and CV were used to monitor the electrochemical performances of immunosensor at different steps of the layer-by-layer procedure of immunosensor fabrication. The electrochemical measurements were conducted in 10 mM $\text{K}_4\text{Fe}(\text{CN})_6/\text{K}_3\text{Fe}(\text{CN})_6$ (1:1 ratio) by using a three-electrode set up including the modified Au electrode (1.5 mm^2 surface area) as working electrode (WE), a Pt wire as an auxiliary electrode (AE), and Ag/AgCl as the reference electrode (RE). The EIS and CV were carried out using an EC-Lab (Bio-Logic, sp-200, Seyssinet-Pariset, France) and a CHI 660C potentiostat (CH Instruments Inc., Austin, TX, USA), respectively. For EIS analysis, a bias voltage of 10 mV was applied between WE and CE over a frequency range of 0.1–1000 Hz. The generated EIS data were fitted to the Randles' equivalent circuit model using ZView software (Solartron Analytical, Farnborough, UK).

2.6. Measurement of *cis* P-tau in PBS and Human Serum

To investigate the electrochemical response of fabricated immunosensor to the different concentrations of *cis* P-tau, the differential pulse voltammetry (DPV) was conducted in 10 mM $\text{K}_4\text{Fe}(\text{CN})_6/\text{K}_3\text{Fe}(\text{CN})_6$ (1:1 ratio) in PBS at pH 7.5. Different solutions of *cis* P-tau in PBS or undiluted human serum with successive concentrations (0×10^{-14} M to 3.0×10^{-9} M) were prepared. The human serum was collected from clotted normal blood and was

used fresh. Prior to the analysis, each *cis* P-tau solution was dropped onto the WE surface, incubated at RT for 30 min, and subsequently washed with PBS.

2.7. Preparation of Real Human Samples

The written informed consent was obtained from all patients and the sample collection protocol was approved by the Ethics Committee of Royan Institute. After the initial survey including mini-mental state examination (MMSE) evaluation, patients underwent CSF sampling. The CSF samples were drained using 20-gauge yellow lumbar puncture needle inserted into the subarachnoid space at the L3–4 or L4–5 interspace after sterile preparation. The 2 to 5 mL of CSF was then collected in sterile plastic tubes for evaluation of biomarker (CSF *cis* P-tau) using an in-house ELISA and the immunosensor. Similarly, for the control group, the CSF sample was drained using the same method at the time of spinal anesthesia and subjected for evaluation of *cis* P-tau. Blood samples were collected from the AD patients at different stages and healthy controls in collaboration with Sasan hospital of Tehran, Iran. Serum samples were derived from the clotted blood and were analyzed fresh. The analysis was carried out blindly according to the clinical status.

2.8. Measurement of *cis* P-tau in Real Samples

The CSF samples were diluted 1/100 in 0.1 M PBS prior to analysis and the serum samples were analyzed without any pretreatment. For immunosensor measurement, each sample was dropped onto the WE surface, incubated at RT for 30 min, washed with PBS, and then, DPV was conducted in 10 mM $K_4Fe(CN)_6/K_3Fe(CN)_6$ (1:1 ratio) in PBS at pH 7.5. To compare with the immunosensor, an in-house ELISA was produced for the detection of *cis* P-tau in real human CSF and serum samples. In brief, 2 μ g of anti *cis*-phosphorylated Thr231-Tau diluted in 100 μ L of PBS (0.01 M, pH 7.2) and was immobilized in 96-well ELISA plates and stored at 4 °C overnight. To reduce nonspecific binding, wells were rinsed with $5 \times 300 \mu$ L Tris-buffered saline/Triton X-100 (TBST) using an automatic plate washer and blocked for 45 min at 37 °C with a blocking solution (TPBS + 0.5 mM BSA). Following additional automated washing, 100 μ L/well of serial standards or human serum were added and incubated at 37 °C for 1 h. Following an additional wash step, 100 μ L of HRP-conjugated goat anti-mouse IgG diluted 1:500 in BSA was added to each well, incubated for 1 h at 37 °C and washed. The colorimetric reaction was initiated upon the addition of 200 μ L of ready-to-use TMB substrate (Seramun Diagnostica GmbH, Germany), and the plates were allowed to rest for 20 min at 37 °C in the dark. Finally, the reaction was stopped with 100 μ L/well of 2 N sulfuric acid, and the absorbance of the samples was determined on a microplate reader at 450 nm (Thermo Fisher Scientific, Waltham, MA, USA). The standard curve was prepared by serial dilution of *cis* P-tau peptide (*cis*-phosphorylated Thr231- Dmp-Tau (KVAVVRpT (5,5-dimethyl-L-proline) PKSPS) in PBS ranging from 0.0001 μ g/mL to 3 μ g/mL. The ELISA assay was performed in triplicate experiments and compared with the results obtained using the immunosensor.

2.9. Statistical Analysis

All statistical analyses were done using Student's *t*-test and $p < 0.05$ was considered to be statistically significant.

3. Results and Discussion

3.1. Fabrication and Characterization of Immunosensor

The topographical changes of the electrode surface during the multi-step procedure of the immunosensor fabrication were monitored using AFM. Figure 2 shows the AFM 3D images at the consequent stages of the sensor fabrication. After deposition of the NHS-activated thiol linkers on the GE, the roughness of the electrode surfaces decreased slightly from 142 nm to 135 nm (Figure 2A,B). Upon addition of the macromolecular agent of the *cis* P-tau antibody, the surface roughness increased dramatically to 144 nm (Figure 2C), which is similar to that observed in other studies [58,59]. Moreover, the addition of analyte, *cis*

P-tau produced a small change in the surface roughness from 144 nm to 148 nm (Figure 2D). The AFM data could confirm the successful deposition of the agents at each stage.

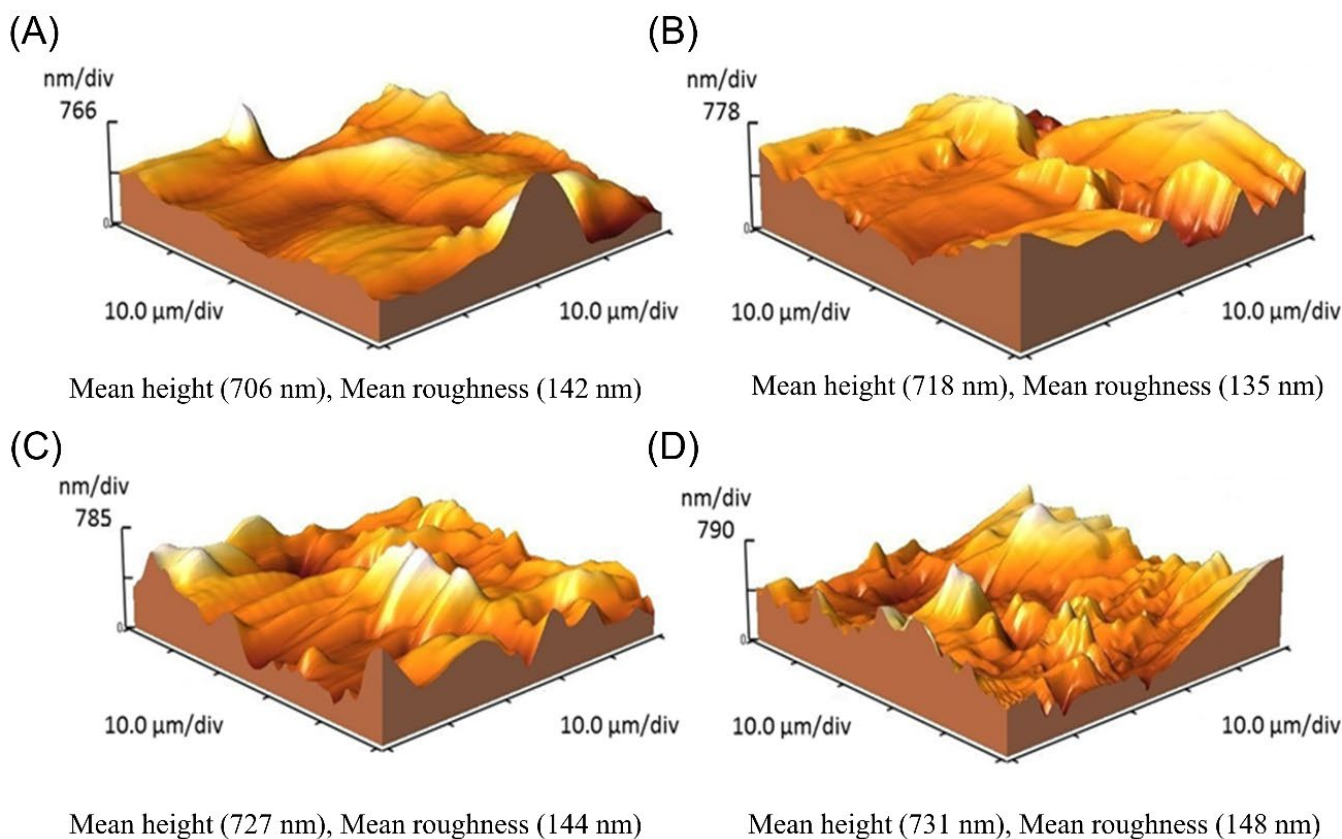


Figure 2. AFM topographic profile of the gold electrode surface in bare state with a roughness of 142 nm (A) and functionalized surface by NHS-activated thiol linkers with a roughness of 135 nm (B), anti-*cis* P-tau-conjugated surface with a roughness of 144 nm (C), and antibody-conjugated surface after the addition of *cis* P-tau with a roughness of 148 nm (D).

EIS and CV were used to confirm the layer-by-layer deposition of substances on the gold electrode surface during the multi-step fabrication process (Figure 3). EIS is a powerful instrument for surface characterization and monitoring changes to the interfaces. The EIS data were showed through Nyquist complex-plane diagrams (Figure 3A). In these diagrams, the semicircle diameter of each impedance spectrum represents the interfacial charge-transfer resistance (R_{ct}) at each step of the immunosensor construction. At the first step, chemical modification of gold surface with MUA/MPA resulted in a remarkable increase in the R_{ct} (1.53 to 7.08 k Ω), which could be related to the lower surface concentration of the probe due to the existence of long carbon chains in the MUA-MPA layer, which could limit the diffusion of $Fe(CN)_6^{3-/4-}$ redox couple towards the electrode surface. Additionally, the peak shift is an indication of the enhancement of difficulty of electron transfer, which was probably caused by the negative charge of the electrode surface via the formation of R-COO⁻ layer. This behavior was realized by a remarkable decrease of the current intensity in CV diagram of the electrode modified with MUA/MPA compared to the bare electrode (Figure 3B). Subsequently, treatment of the MUA/MPA-modified electrode by EDC/NHS showed a declined R_{ct} (2.16 k Ω) and an increased current intensity in CV (Figure 3B). This could contribute to the elimination of the negative charges through NHS ester formation on the carboxylic groups, which generally reduces the negative charges of the electrode surface and facilities the probe diffusion ability. These results confirmed that the CO₂⁻ groups of MUA/MPA were activated with NHS coupling. Upon the immobilization of *cis* P-tau mAb on the activated gold electrode, a remarkable increase in the R_{ct} (3.28 k Ω) and decrease in the current intensity (Figure 3B) were observed due to the binding and

accumulation of the macromolecular antibody on the electrode surface which may cause more blockage in the diffusion path of the probe ions towards the electrode surface. The results of EIS and CV were in agreement and confirmed the success of the layer-by-layer assembly process during fabrication and performance of the immunosensor. Upon addition of *cis* P-tau solution onto the electrode surface, the peak current was further decreased, suggesting the successful recognition of *cis* P-tau by the antibody and accumulation of the *cis* P-tau macromolecules on the electrode which can hinder electron transfer between the electrode surface and the solution containing the $[\text{Fe}(\text{CN})_6]^{3-/4-}$ redox probe. All the measurements were conducted under pH 7.5, which was determined as the optimal pH of medium for maximal electrochemical signal production in response to *cis* P-tau (Figure S1).

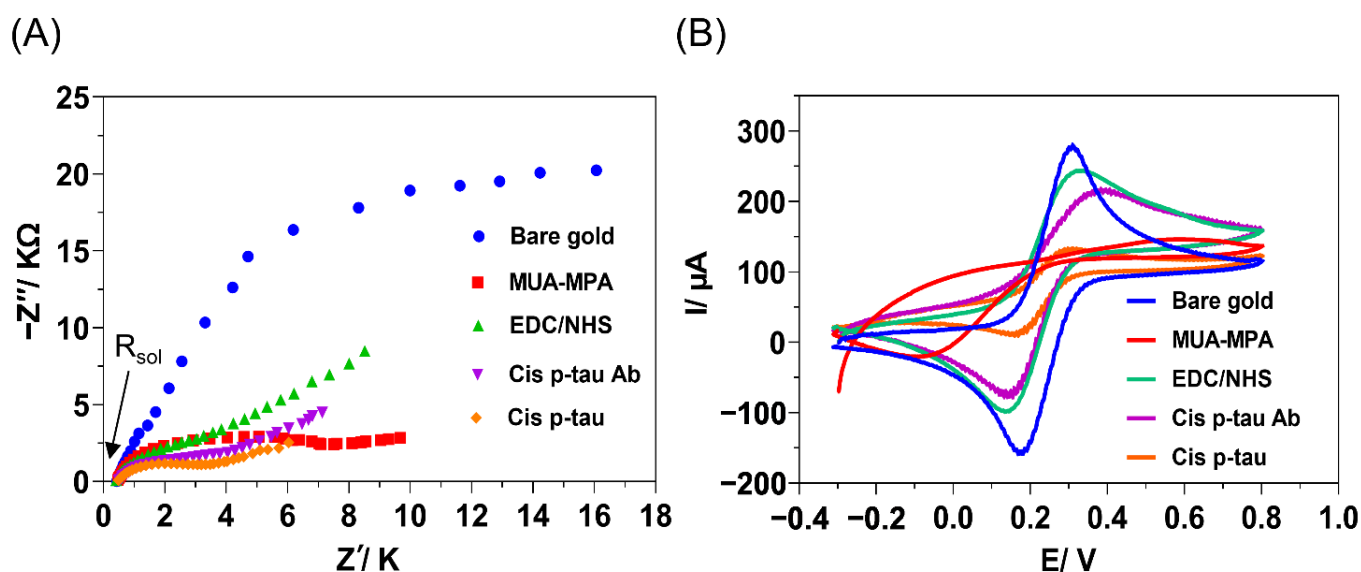


Figure 3. Electrochemical monitoring of the layer-by-layer assembly process carried out for fabrication of immunosensor, including the cleaned bare gold (blue), chemical modification with linkers MUA/MPA (red), activation of linkers with EDC/NHS (green), immobilization of *cis* P-tau mAb (Purple), and deposition of *cis* P-tau (orange). **(A)** Electrochemical impedance spectroscopy (EIS). The imaginary component of EIS (Z'') was plotted against the real component of EIS (Z') in a Nyquist plot (resistance of solution, $R_{\text{sol}} = 33 \Omega$). **(B)** Cyclic voltammetry (CV) voltammogram. The electrochemical measurements were conducted in PBS (pH 7.5) containing 10 mM $\text{K}_4\text{Fe}(\text{CN})_6/\text{K}_3\text{Fe}(\text{CN})_6$ (1:1 ratio) by using a three-electrode set up including the modified Au surface as working electrode, a Pt wire as an auxiliary electrode, and Ag/AgCl as the reference electrode.

3.2. Selectivity of Immunosensor

To investigate the selectivity of the immunosensor to *cis* P-tau, the possibility of an off-target response to *trans* P-tau and major plasma proteins including albumin, beta-2-microglobulin, immunoglobulin G, and hemoglobin was studied by DPV analysis (Figure 4). These proteins were chosen as major off-targets because *trans* P-tau is the other isomer of P-tau, which is not considered as early driver of AD, albumin and beta-2-microglobulin are abundant in CSF and serum and beta-2-microglobulin is routinely tested as a representative of the heavy inflammatory marker proteins in CSF, IgG is an immunoprotein that is elevated in CSF in cases of infection, and hemoglobin is routinely tested as a blood protein [60–64]. The presence of these components in biological fluids may interfere with detection of low abundant biomarkers in clinical samples [65]. The immunosensor response to these proteins was analyzed by DPV method (Figure 4A), and the current intensity change upon incubation with each protein was measured from five independent experiments (Figure 4B). The data showed that upon incubation with the off-target proteins, the recorded signal was similar to the blank PBS, while a sharp signal rise was observed with the target protein *cis* P-tau even at lower concentration. The result affirmed that no considerable

non-selective binding occurred between anti-*cis* P-tau antibody and the off-target proteins and the produced signal with incubation of *cis* P-tau was the result of specific antibody–antigen interactions. This specificity against the *cis* isomer of P-tau was further confirmed by analysis of signal production in response to higher concentrations of *trans* P-tau (100, 1000, and 2000 pM), which showed no significant signal change at all the levels of this off-target isomer (Figure S2).

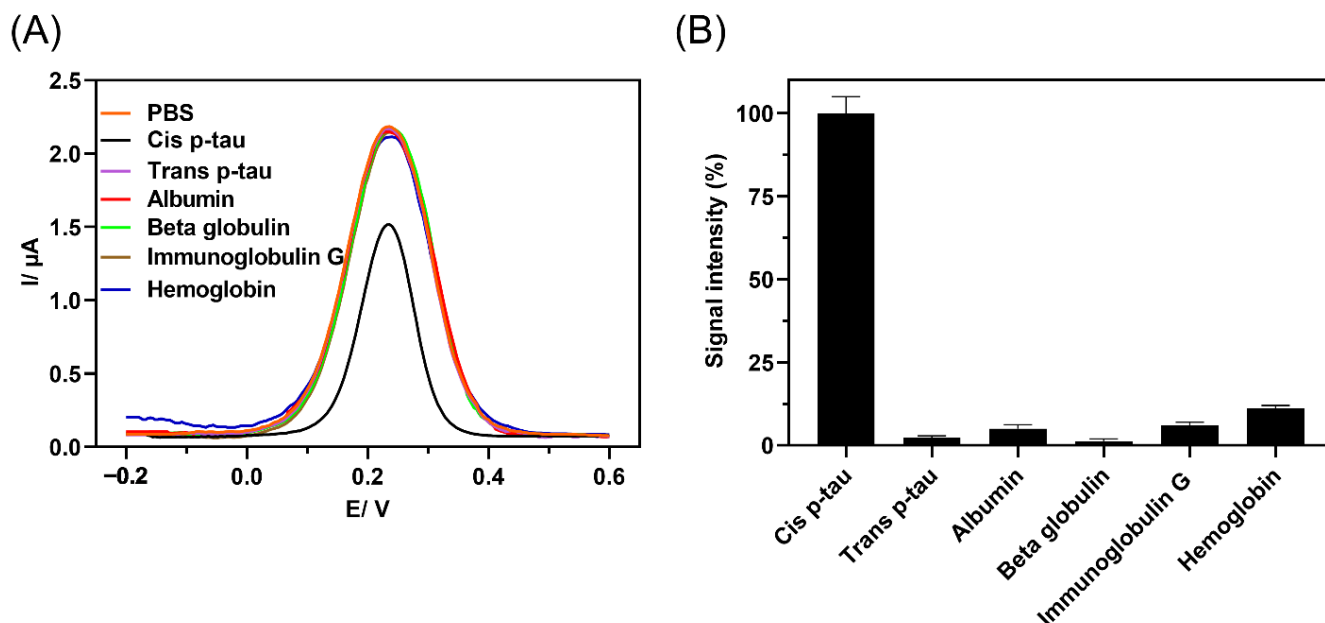


Figure 4. A comparison of DPV response to *cis* P-tau (1.0×10^{-12} M) and possible off-targets, including *trans* P-tau (40×10^{-12} M) and major plasma proteins, albumin (1.0×10^{-9} M), beta-2-microglobulin (1.0×10^{-9} M), immunoglobulin G (IgG) (1.0×10^{-9} M), and hemoglobin (1.0×10^{-9} M). (A) The signal intensity produced by immunosensor in response to protein solutions in PBS containing 10 mM $\text{K}_4\text{Fe}(\text{CN})_6/\text{K}_3\text{Fe}(\text{CN})_6$ (1:1 ratio) was analyzed by DPV method and (B) the immunosensor specificity was measured by relative signal intensity with respect to the baseline ($\%I_R$), $\%I_R = (I_{\text{Bare}} - I_{\text{Protein}})/I_{\text{Bare}} \times 100$, where I_{Bare} represents the current intensity of the blank immunosensor and I_{Protein} represents the current intensity of the immunosensor upon incubation with each protein ($n = 5$). The larger the relative current signal difference ($\%I_R$), the greater the protein recognition.

3.3. Characterization of the Immunosensor Response to *cis* P-tau in PBS and Human Serum

After exploring and determining various optimal experimental conditions, the analytical performance of this immunosensor was evaluated by DPV measurements. Firstly, the matrix effect on the current response of immunosensor was studied by analyzing different blank matrices, PBS, serum, and CSF. The current responses were acquired upon the addition of *cis* P-tau with successive concentration (5.0×10^{-14} M to 3.0×10^{-9} M) to PBS or human serum (Figure 5). Upon addition of *cis* P-tau, the peak current decreased compared with the blank in a concentration-dependent manner (Figure 5A,B). The current response suppression at different concentrations of *cis* P-tau was calculated from the DPV analysis and plotted in Figure 5C,D. A linear relationship was found between the current change and the *cis* P-tau concentration at the range of 5.0×10^{-14} M to 5.0×10^{-10} M (insets in Figure 5C,D), with the correlation coefficients more than 0.99 for both PBS and serum samples. At a $\text{SNR} \geq 3$, the limits of detection (LOD) were calculated to be 2.0×10^{-14} M and 5.0×10^{-14} M, for PBS and human serum samples, respectively. The obtained LOD was comparable with the electrochemical sensors which have been developed previously for tau protein [17,29,66]. These observations evidenced high sensitivity of the immunosensor for measurement of *cis* P-tau, either in PBS or a complex matrix such as serum.

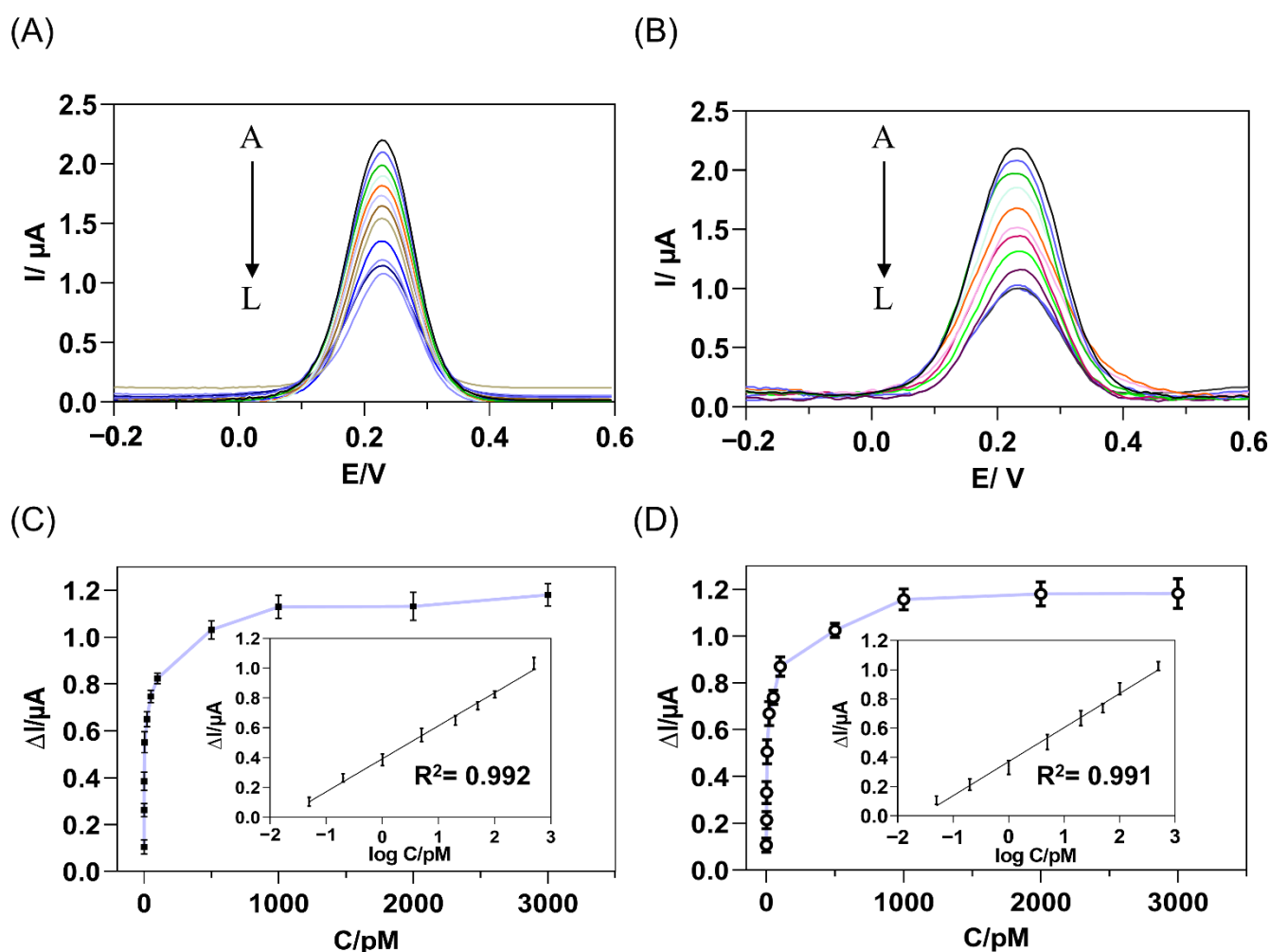


Figure 5. DPV response of the immunosensor to the increasing concentrations of target *cis* P-tau, from A to L: 0, 0.05, 0.2, 1, 5, 20, 50, 100, 500, 1000, 2000, 3000 pM, added to PBS (A) or human serum (B) containing the $[\text{Fe}(\text{CN})_6]^{3-/4-}$ as a redox probe. The relationship between the current response suppression and *cis* P-tau concentration was calculated from the DPV analysis of PBS (C) and human serum (D) samples. The insets show the linear calibration curve of the DPV current decrease versus the logarithm of complementary *cis* P-tau concentration (D) and the error bars represent standard deviations of the measurements ($n = 3$). The regression equation was obtained as $\Delta I (\mu\text{A}) = 0.2136 + 0.4042 \log C (\text{pM})$ and $\Delta I (\mu\text{A}) = 0.23326 + 0.3713 \log C (\text{pM})$ for PBS and human serum samples, respectively, where ΔI is the current decrement and C is the concentration of *cis* P-tau.

3.4. Clinical Applicability of the Immunosensor for Analysis of Real Samples

To investigate the applicability of our immunosensor in real clinical settings, we used it to detect *cis* P-tau in CSF and serum samples collected from human patients. The *cis* P-tau in real human CSF of healthy and different stages of AD (MCI and dementia) could be detected by the immunosensor in good agreement with the ELISA assay (Table 1). In addition, the standard addition method was used to investigate the sensitivity of the immunosensor to linear changes of the analyte level in the real sample [67,68]. To this end, *cis* P-tau was added to the real CSF samples with subsequent concentrations and the produced DPV signal was acquired (Table S1 and Figure S3). The added standards were recovered in the range from 97.9 to 106.3% with a high repeatability (RSD < 5.5%), showing the acceptable sensitivity of the immunosensor for detection of small changes of *cis* P-tau level in real samples.

Table 1. Determination of *cis* P-tau in real human CSF samples collected from healthy and diseased subjects by using immunosensor and an in-house ELISA.

Sample	<i>cis</i> P-tau Concentration (pM)				<i>p</i> -Value ^c
	ELISA ^a	Immunosensor ^a	ELISA ^b	Immunosensor ^b	
Healthy	15.3 ± 1.2	15.0 ± 0.8	13.9–16.7	14.1–15.9	0.57
MCI	60.3 ± 2.0	59.0 ± 2.2	58.0–62.6	56.5–61.5	0.63
Dementia	80.7 ± 1.7	82.3 ± 1.24	78.7–82.6	80.9–83.7	0.21

^a Mean ± standard deviation (*n* = 3); ^b confidence interval at 95% level; ^c calculated by Student's *t*-test.

In clinical practice, blood samples are more preferable than the CSF samples that are obtained invasively from the patients, especially when a frequent screening program is desired for early detection among high-risk candidates. Although classic approaches such as ELISA can be established to detect *cis* P-tau in CSF (cut-off ~ 10–20 pM) by using our mAb, their sensitivity and selectivity is much lower to determine the extremely lower levels of P-tau in complex samples of blood serum [53]. In our experiences with the in-house ELISA, serum detection was not possible at any stages of AD (data not shown). Moreover, ELISA is a label-based technique with clinical applicability that is challenging due to the costly and time-consuming step of analyte labeling with the signal tags. However, the label-free electrochemical detection mechanism of the immunosensor allows for easy, fast, and cost-effective analysis which potentiate its clinical applicability. The immunosensor measurement of *cis* P-tau in the serum samples of healthy and Alzheimer's subjects at different stages of AD successfully detected *cis* P-tau at higher levels in AD samples compared with the healthy samples (Table 2). Notably, the *cis* P-tau was detected at levels correlated with the disease stages which suggests the applicability of the immunosensor for serum detection of AD, even at the earlier stages. This label-free detection mechanism allows for easy, fast, and cost-effective analysis without the need for labeling the analyte with the signal tags that are common in classic methods such as ELISA.

Table 2. Determination of *cis* P-tau in real human serum samples collected from healthy and diseased subjects by using immunosensor.

Sample	<i>cis</i> P-tau Concentration (pM) *	RSD (%)
Healthy	0.02 ± 0.0011	5.5
MCI	0.05 ± 0.0025	5.0
Dementia-1	0.18 ± 0.0080	4.4
Dementia-2	2.0 ± 0.0800	4.0
Dementia-3	3.1 ± 0.1085	3.5

* Mean ± standard deviation (*n* = 3).

In order to evaluate the stability of the immunosensor during long-term storage in clinical practice, the immunosensors were stored at 4 °C and their responses to *cis* P-tau (10 pM) were recorded over a period of 90 days (Figure S4). The results showed a slight attenuation trend during storage, so that the amount of current produced on day 90 decreased by only 3.5% compared to the first day. Therefore, the immunosensor can support an acceptable shelf-life which is crucial for application in clinical services.

4. Conclusions

In this study, we utilized a proprietary antibody against *cis* P-tau to develop a novel electrochemical immunosensor for the detection of *cis* P-tau as an early biomarker of AD. The immunosensor was fabricated by covalent immobilization of anti-*cis* P-tau mAb onto a gold electrode surface by using a combination of NHS-activated thiol linkers. By using DPV electrochemical analysis, the *cis* P-tau was detected in PBS and human serum matrices with subsequent concentrations up to 0.02 and 0.05 pM, respectively. The immunosensor performed successfully in the real situation as the *cis* P-tau was measured in human pa-

tient CSF samples in good agreement with an in-house ELISA and recovered precisely in manually spiked CSF samples. More importantly, the immunosensor detection was successful in human serum samples collected from AD patients at different disease stages with a low cut-off (0.05 pM), while the detection was not possible with the ELISA. The focus on a specific isomer of P-tau, which is the major early driver of AD, is the main superiority of this work than the previous works on AD detection based on tau measurement (Table 3). As cistausis is a well-known early driver of tauopathy in several neurodegenerative diseases such as AD, this immunosensor may find a unique clinical application in early diagnostic procedures.

Table 3. A comparison between this work and similar works on AD detection based on tau measurement.

Method	Analyte	LOD	Sample	Labeling	Reference
Electrochemical	Tau	0.2 μ M	BSA	Label-free	[20]
Electrochemical	Tau	1000 pg/mL, 100,000 pg/mL	PBS, Serum	Label-free	[23]
Electrochemical	Tau	<1 pM	CSF	Label-free	[24]
Electrochemical	Tau-381	0.42 pM	Serum	Labeled	[21]
Photoelectrochemical	Tau-381	0.3 fM	Serum	Labeled	[69]
Electrochemical	full-length 2N4R tau	0.03 pM	Serum	Label-free	[17]
Impedimetric	Tau-441	0.091 pg/mL	Serum, CSF	Labeled	[70]
Electrochemical	P-tau-441	0.02 pM	PBS	Label-free	[71]
Electrochemical	cis pT231-tau	0.02 pM, 0.05 pM	PBS, CSF, Serum	Label-free	

Supplementary Materials: The following supporting information can be downloaded at: <https://www.mdpi.com/article/10.3390/bios12100879/s1>, Figure S1. Response characterization of immunosensor to *cis* p-tau in PBS (1.0×10^{-12} M) at different pH values of the solution containing the 10 mM $K_4Fe(CN)_6/K_3Fe(CN)_6$ (1:1 ratio), analyzed by DPV method ($n = 3$); Figure S2. The DPV response of immunosensor to different concentrations of *trans* p-tau in 0.1 M PBS containing 10 mM of $[Fe(CN)_6]^{3-}/4-$ as a redox probe; Figure S3. DPV response of the immunosensor to added standard solutions of *cis* p-tau to human CSF samples obtained from healthy and Alzheimer's individuals at different stages of AD ($n = 3$); Figure S4. Comparison of immunosensor DPV response to *cis* p-tau in PBS (10×10^{-12} M) after immunosensor storage at 4 °C over a 90 days period ($n = 9$); Table S1. Precision (RSD%) and recovery study of the immunosensor performed by adding standard solutions of *cis* p-tau to human CSF samples obtained from healthy and Alzheimer's individuals at different stages of AD ($n = 3$).

Author Contributions: Conceptualization, A.S., M.K.A., M.-H.G. and F.F.; methodology, A.S., F.Y., M.K.A., M.-H.G. and F.F.; software, A.S., F.Y. and M.-H.G.; validation, F.Y., K.S. and F.F.; formal analysis, A.S., F.Y., N.T. and F.F.; investigation, A.S., M.K.A., M.-H.G., K.S. and F.S.; resources, A.S. and F.F.; data curation, M.K.A., M.-H.G., F.S. and F.F.; writing—original draft preparation, A.S.; writing—review and editing, M.K.A., M.-H.G. and F.F.; visualization, A.S.; supervision, F.S.; project administration, M.K.A., M.-H.G., F.S. and F.F.; funding acquisition, F.S. All authors have read and agreed to the published version of the manuscript.

Funding: This work was financially supported by a grant from Cognitive Sciences and Technologies Council (CSTC, Grant No. 6296) to F.S.

Institutional Review Board Statement: The study was conducted in accordance with the Declaration of Helsinki, and approved by the Institutional Review Board (or Ethics Committee) of Royan institute (IR.ACECR.ROYAN.REC.1397.221).

Informed Consent Statement: Informed consent was obtained from all subjects involved in the study.

Data Availability Statement: Data is contained within the article and Supplementary Material.

Acknowledgments: The human real samples were kindly provided by medical diagnostic laboratories of Sasan Hospital and Iran University of Medical Sciences.

Conflicts of Interest: The authors declare no conflict of interest.

References

1. Srivastava, S.; Ahmad, R.; Khare, S.K. Alzheimer's disease and its treatment by different approaches: A review. *Eur. J. Med. Chem.* **2021**, *216*, 113320. [[CrossRef](#)] [[PubMed](#)]
2. Hampel, H.; Prvulovic, D.; Teipel, S.; Jessen, F.; Luckhaus, C.; Frölich, L.; Riepe, M.W.; Dodel, R.; Leyhe, T.; Bertram, L. The future of Alzheimer's disease: The next 10 years. *Prog. Neurobiol.* **2011**, *95*, 718–728. [[CrossRef](#)] [[PubMed](#)]
3. Rochoy, M.; Rivas, V.; Chazard, E.; Decarpentry, E.; Saudemont, G.; Hazard, P.-A.; Puisieux, F.; Gautier, S.; Bordet, R. Factors associated with Alzheimer's disease: An overview of reviews. *J. Prev. Alzheimer's Dis.* **2019**, *6*, 121–134. [[CrossRef](#)] [[PubMed](#)]
4. Alzheimer's Association. 2018 Alzheimer's disease facts and figures. *Alzheimer's Dement.* **2018**, *14*, 367–429. [[CrossRef](#)]
5. Maiese, K. MicroRNAs for the Treatment of Dementia and Alzheimer's Disease. *Curr. Neurovascular Res.* **2019**, *16*, 1–2. [[CrossRef](#)]
6. Lee, C.M.; Woodward, M.; Batty, G.D.; Beiser, A.S.; Bell, S.; Berr, C.; Bjertness, E.; Chalmers, J.; Clarke, R.; Dartigues, J.F. Association of anthropometry and weight change with risk of dementia and its major subtypes: A meta-analysis consisting 2.8 million adults with 57 294 cases of dementia. *Obes. Rev.* **2020**, *21*, e12989. [[CrossRef](#)]
7. Lee, J.C.; Kim, S.J.; Hong, S.; Kim, Y. Diagnosis of Alzheimer's disease utilizing amyloid and tau as fluid biomarkers. *Exp. Mol. Med.* **2019**, *51*, 1–10. [[CrossRef](#)]
8. Miley-Akerstedt, A.; Jelic, V.; Marklund, K.; Waller, H.; Åkerstedt, T.; Hagman, G.; Andersson, C. Lifestyle factors are important contributors to subjective memory complaints among patients without objective memory impairment or positive neurochemical biomarkers for Alzheimer's disease. *Dement. Geriatr. Cogn. Disord. Extra* **2018**, *8*, 439–452. [[CrossRef](#)]
9. Rajasekhar, K.; Govindaraju, T. Current progress, challenges and future prospects of diagnostic and therapeutic interventions in Alzheimer's disease. *RSC Adv.* **2018**, *8*, 23780–23804. [[CrossRef](#)]
10. Zetterberg, H.; Bendlin, B.B. Biomarkers for Alzheimer's disease—Preparing for a new era of disease-modifying therapies. *Mol. Psychiatry* **2021**, *26*, 296–308. [[CrossRef](#)]
11. Aisen, P.S.; Jimenez-Maggiara, G.A.; Rafii, M.S.; Walter, S.; Raman, R. Early-stage Alzheimer disease: Getting trial-ready. *Nat. Rev. Neurol.* **2022**, *18*, 389–399. [[CrossRef](#)] [[PubMed](#)]
12. Tao, Y.; Han, Y.; Yu, L.; Wang, Q.; Leng, S.X.; Zhang, H. The Predicted key molecules, functions, and pathways that bridge Mild Cognitive Impairment (MCI) and Alzheimer's Disease (AD). *Front. Neurol.* **2020**, *11*, 233. [[CrossRef](#)] [[PubMed](#)]
13. Blennow, K.; Zetterberg, H. Biomarkers for Alzheimer's disease: Current status and prospects for the future. *J. Intern. Med.* **2018**, *284*, 643–663. [[CrossRef](#)] [[PubMed](#)]
14. Hassan, Q.; Kerman, K. Electrochemical approaches for the detection of amyloid- β , tau, and α -synuclein. *Curr. Opin. Electrochem.* **2019**, *14*, 89–95. [[CrossRef](#)]
15. Lin-Yu, L.; Xiao-Ying, W. Progress in Analysis of Tau Protein. *Chin. J. Anal. Chem.* **2020**, *48*, 685–694.
16. Shui, B.; Tao, D.; Florea, A.; Cheng, J.; Zhao, Q.; Gu, Y.; Li, W.; Jaffrezic-Renault, N.; Mei, Y.; Guo, Z. Biosensors for Alzheimer's disease biomarker detection: A review. *Biochimie* **2018**, *147*, 13–24. [[CrossRef](#)]
17. Wang, S.X.; Acha, D.; Shah, A.J.; Hills, F.; Roitt, I.; Demosthenous, A.; Bayford, R.H. Detection of the tau protein in human serum by a sensitive four-electrode electrochemical biosensor. *Biosens. Bioelectron.* **2017**, *92*, 482–488. [[CrossRef](#)]
18. Razzino, C.A.; Serafín, V.; Gamella, M.; Pedrero, M.; Montero-Calle, A.; Barderas, R.; Calero, M.; Lobo, A.O.; Yáñez-Sedeño, P.; Campuzano, S. An electrochemical immunosensor using gold nanoparticles-PAMAM-nanostructured screen-printed carbon electrodes for tau protein determination in plasma and brain tissues from Alzheimer patients. *Biosens. Bioelectron.* **2020**, *163*, 112238. [[CrossRef](#)]
19. Carlin, N.; Martic-Milne, S. Anti-tau antibodies based electrochemical sensor for detection of tau protein biomarkers. *J. Electrochem. Soc.* **2018**, *165*, G3018. [[CrossRef](#)]
20. Esteves-Villanueva, J.O.; Trzeciakiewicz, H.; Martic, S. A protein-based electrochemical biosensor for detection of tau protein, a neurodegenerative disease biomarker. *Analyst* **2014**, *139*, 2823–2831. [[CrossRef](#)]
21. Shui, B.; Tao, D.; Cheng, J.; Mei, Y.; Jaffrezic-Renault, N.; Guo, Z. A novel electrochemical aptamer-antibody sandwich assay for the detection of tau-381 in human serum. *Analyst* **2018**, *143*, 3549–3554. [[CrossRef](#)] [[PubMed](#)]
22. Muralidar, S.; Ambi, S.V.; Sekaran, S.; Thirumalai, D.; Palaniappan, B. Role of tau protein in Alzheimer's disease: The prime pathological player. *Int. J. Biol. Macromol.* **2020**, *163*, 1599–1617. [[CrossRef](#)] [[PubMed](#)]
23. Dai, Y.; Molazemhosseini, A.; Liu, C.C. A single-use, in vitro biosensor for the detection of T-tau protein, a biomarker of neurodegenerative disorders, in PBS and human serum using differential pulse voltammetry (DPV). *Biosensors* **2017**, *7*, 10. [[CrossRef](#)] [[PubMed](#)]
24. García-Chamé, M.-Á.; Gutiérrez-Sanz, Ó.; Ercan-Herbst, E.; Hausteiner, N.; Filipiak, M.S.; Ehrnhöfer, D.E.; Tarasov, A. A transistor-based label-free immunosensor for rapid detection of tau protein. *Biosens. Bioelectron.* **2020**, *159*, 112129. [[CrossRef](#)]
25. Ameri, M.; Shabaninejad, Z.; Movahedpour, A.; Sahebkar, A.; Mohammadi, S.; Hosseindoost, S.; Ebrahimi, M.S.; Savardashtaki, A.; Karimipour, M.; Mirzaei, H. Biosensors for detection of Tau protein as an Alzheimer's disease marker. *Int. J. Biol. Macromol.* **2020**, *162*, 1100–1108. [[CrossRef](#)] [[PubMed](#)]
26. Song, Y.; Xu, T.; Zhu, Q.; Zhang, X. Integrated individually electrochemical array for simultaneously detecting multiple Alzheimer's biomarkers. *Biosens. Bioelectron.* **2020**, *162*, 112253. [[CrossRef](#)]

27. Kim, S.; Wark, A.W.; Lee, H.J. Femtomolar detection of tau proteins in undiluted plasma using surface plasmon resonance. *Anal. Chem.* **2016**, *88*, 7793–7799. [[CrossRef](#)]
28. Ahmadi, S.; Ebralidze, I.I.; She, Z.; Kraatz, H.-B. Electrochemical studies of tau protein-iron interactions—Potential implications for Alzheimer’s Disease. *Electrochim. Acta* **2017**, *236*, 384–393. [[CrossRef](#)]
29. Han, Q.; Pang, J.; Li, Y.; Sun, B.; Ibarlucea, B.; Liu, X.; Gemming, T.; Cheng, Q.; Zhang, S.; Liu, H. Graphene Biodevices for Early Disease Diagnosis Based on Biomarker Detection. *ACS Sens.* **2021**, *6*, 3841–3881. [[CrossRef](#)]
30. Chong, J.R.; Ashton, N.J.; Karikari, T.K.; Tanaka, T.; Schöll, M.; Zetterberg, H.; Blennow, K.; Chen, C.P.; Lai, M.K. Blood-based high sensitivity measurements of beta-amyloid and phosphorylated tau as biomarkers of Alzheimer’s disease: A focused review on recent advances. *J. Neurol. Neurosurg. Psychiatry* **2021**, *92*, 1231–1241. [[CrossRef](#)]
31. Ma, R.-H.; Zhang, Y.; Hong, X.-Y.; Zhang, J.-F.; Wang, J.-Z.; Liu, G.-P. Role of microtubule-associated protein tau phosphorylation in Alzheimer’s disease. *J. Huazhong Univ. Sci. Technol. Med. Sci.* **2017**, *37*, 307–312. [[CrossRef](#)] [[PubMed](#)]
32. Mietelska-Porowska, A.; Wasik, U.; Goras, M.; Filipek, A.; Niewiadomska, G. Tau protein modifications and interactions: Their role in function and dysfunction. *Int. J. Mol. Sci.* **2014**, *15*, 4671–4713. [[CrossRef](#)] [[PubMed](#)]
33. Kontsekova, E.; Zilka, N.; Kovacech, B.; Novak, P.; Novak, M. First-in-man tau vaccine targeting structural determinants essential for pathological tau–tau interaction reduces tau oligomerisation and neurofibrillary degeneration in an Alzheimer’s disease model. *Alzheimer’s Res. Ther.* **2014**, *6*, 44. [[CrossRef](#)] [[PubMed](#)]
34. Šimić, G.; Babić Leko, M.; Wray, S.; Harrington, C.; Delalle, I.; Jovanov-Milošević, N.; Bažadona, D.; Buée, L.; De Silva, R.; Di Giovanni, G. Tau protein hyperphosphorylation and aggregation in Alzheimer’s disease and other tauopathies, and possible neuroprotective strategies. *Biomolecules* **2016**, *6*, 6. [[CrossRef](#)]
35. Albayram, O.; Herbert, M.K.; Kondo, A.; Tsai, C.-Y.; Baxley, S.; Lian, X.; Hansen, M.; Zhou, X.Z.; Lu, K.P. Function and regulation of tau conformations in the development and treatment of traumatic brain injury and neurodegeneration. *Cell Biosci.* **2016**, *6*, 59. [[CrossRef](#)]
36. Kondo, A.; Shahpasand, K.; Mannix, R.; Qiu, J.; Moncaster, J.; Chen, C.-H.; Yao, Y.; Lin, Y.-M.; Driver, J.A.; Sun, Y. Antibody against early driver of neurodegeneration cis P-tau blocks brain injury and tauopathy. *Nature* **2015**, *523*, 431–436. [[CrossRef](#)]
37. Khodarahmi, R.; Akbari, V.; Mohammadi, S.; Farshadnia, T.; Rahimabadi, M.M.; Goicoechea, H.C.; Jalalvand, A.R. Chemometric modeling of the electrochemical data to investigate proline cis/trans isomerisation effect on aggregation of Tau protein. *Protein Expr. Purif.* **2021**, *182*, 105858. [[CrossRef](#)]
38. Nakamura, K.; Greenwood, A.; Binder, L.; Bigio, E.H.; Denial, S.; Nicholson, L.; Zhou, X.Z.; Lu, K.P. Proline isomer-specific antibodies reveal the early pathogenic tau conformation in Alzheimer’s disease. *Cell* **2012**, *149*, 232–244. [[CrossRef](#)]
39. Hajipour, M.J.; Santoso, M.R.; Rezaee, F.; Aghaverdi, H.; Mahmoudi, M.; Perry, G. Advances in Alzheimer’s diagnosis and therapy: The implications of nanotechnology. *Trends Biotechnol.* **2017**, *35*, 937–953. [[CrossRef](#)]
40. Naserkhaki, R.; Zamanzadeh, S.; Baharvand, H.; Nabavi, S.M.; Pakdaman, H.; Shahbazi, S.; Vosough, M.; Ghaedi, G.; Barzegar, A.; Mirtorabi, D. cis pT231-tau drives neurodegeneration in bipolar disorder. *ACS Chem. Neurosci.* **2019**, *10*, 1214–1221. [[CrossRef](#)]
41. Pourhamzeh, M.; Joghataei, M.T.; Mehrabi, S.; Ahadi, R.; Hojjati, S.M.M.; Fazli, N.; Nabavi, S.M.; Pakdaman, H.; Shahpasand, K. The Interplay of Tau Protein and β -Amyloid: While Tauopathy Spreads More Profoundly Than Amyloidopathy, Both Processes Are Almost Equally Pathogenic. *Cell Mol. Neurobiol.* **2021**, *41*, 1339–1354. [[CrossRef](#)] [[PubMed](#)]
42. Sandusky-Beltran, L.; Sigurdsson, E. Tau immunotherapies: Lessons learned, current status and future considerations. *Neuropharmacology* **2020**, *175*, 108104. [[CrossRef](#)] [[PubMed](#)]
43. Lu, P.-J.; Wulf, G.; Zhou, X.Z.; Davies, P.; Lu, K.P. The prolyl isomerase Pin1 restores the function of Alzheimer-associated phosphorylated tau protein. *Nature* **1999**, *399*, 784–788. [[CrossRef](#)]
44. Zhou, X.Z.; Kops, O.; Werner, A.; Lu, P.-J.; Shen, M.; Stoller, G.; Küllertz, G.; Stark, M.; Fischer, G.; Lu, K.P. Pin1-dependent prolyl isomerization regulates dephosphorylation of Cdc25C and tau proteins. *Mol. Cell* **2000**, *6*, 873–883. [[CrossRef](#)]
45. Liou, Y.-C.; Sun, A.; Ryo, A.; Zhou, X.Z.; Yu, Z.-X.; Huang, H.-K.; Uchida, T.; Bronson, R.; Bing, G.; Li, X. Role of the prolyl isomerase Pin1 in protecting against age-dependent neurodegeneration. *Nature* **2003**, *424*, 556–561. [[CrossRef](#)] [[PubMed](#)]
46. Caldwell, J.Z.; Cummings, J.L.; Banks, S.J.; Palmqvist, S.; Hansson, O. Cognitively normal women with Alzheimer’s disease proteinopathy show relative preservation of memory but not of hippocampal volume. *Alzheimer’s Res. Ther.* **2019**, *11*, 109. [[CrossRef](#)]
47. Lleó, A.; Alcolea, D.; Martínez-Lage, P.; Scheltens, P.; Parnetti, L.; Poirier, J.; Simonsen, A.H.; Verbeek, M.M.; Rosa-Neto, P.; Slot, R.E. Longitudinal cerebrospinal fluid biomarker trajectories along the Alzheimer’s disease continuum in the BIOMARKAPD study. *Alzheimer’s Dement.* **2019**, *15*, 742–753. [[CrossRef](#)]
48. Luna-Munoz, J.; Chavez-Macias, L.; Garcia-Sierra, F.; Mena, R. Earliest Stages of Tau Conformational Changes are Related to the Appearance of a Sequence of Specific Phospho-Dependent Tau Epitopes in Alzheimer’s Disease 1. *J. Alzheimer’s Dis.* **2007**, *12*, 365–375. [[CrossRef](#)]
49. Lee, T.H.; Pastorino, L.; Lu, K.P. Peptidyl-prolyl cis–trans isomerase Pin1 in ageing, cancer and Alzheimer disease. *Expert Rev. Mol. Med.* **2011**, *13*, E21. [[CrossRef](#)]
50. Zhang, L.; Liang, X.; Zhang, Z.; Luo, H. Cerebrospinal fluid and blood biomarkers in the diagnostic assays of Alzheimer’s disease. *J. Innov. Opt. Health Sci.* **2021**, *15*, 2230001. [[CrossRef](#)]

51. Sato, C.; Barthélemy, N.R.; Mawuenyega, K.G.; Patterson, B.W.; Gordon, B.A.; Jockel-Balsarotti, J.; Sullivan, M.; Crisp, M.J.; Kasten, T.; Kirmess, K.M. Tau kinetics in neurons and the human central nervous system. *Neuron* **2018**, *97*, 1284–1298. [\[CrossRef\]](#) [\[PubMed\]](#)
52. Shi, M.; Sui, Y.-T.; Peskind, E.R.; Li, G.; Hwang, H.; Devic, I.; Gingham, C.; Edgar, J.S.; Pan, C.; Goodlett, D.R. Salivary tau species are potential biomarkers of Alzheimer's disease. *J. Alzheimer's Dis.* **2011**, *27*, 299–305. [\[CrossRef\]](#)
53. d'Abramo, C.; Acker, C.M.; Schachter, J.B.; Terracina, G.; Wang, X.; Forest, S.K.; Davies, P. Detecting tau in serum of transgenic animal models after tau immunotherapy treatment. *Neurobiol. Aging* **2016**, *37*, 58–65. [\[CrossRef\]](#) [\[PubMed\]](#)
54. Qiu, C.; Albayram, O.; Kondo, A.; Wang, B.; Kim, N.; Arai, K.; Tsai, C.-Y.; Bassal, M.A.; Herbert, M.K.; Washida, K. Cis P-tau underlies vascular contribution to cognitive impairment and dementia and can be effectively targeted by immunotherapy in mice. *Sci. Transl. Med.* **2021**, *13*, eaaz7615. [\[CrossRef\]](#) [\[PubMed\]](#)
55. Albayram, O.; Kondo, A.; Mannix, R.; Smith, C.; Tsai, C.-Y.; Li, C.; Herbert, M.K.; Qiu, J.; Monuteaux, M.; Driver, J. Cis P-tau is induced in clinical and preclinical brain injury and contributes to post-injury sequelae. *Nat. Commun.* **2017**, *8*, 1000. [\[CrossRef\]](#)
56. Roqanian, S.; Ahmadian, S.; Nabavi, S.M.; Pakdaman, H.; Shafiezhadeh, M.; Goudarzi, G.; Shahpasand, K. Tau nuclear translocation is a leading step in tau pathology process through P53 stabilization and nucleolar dispersion. *J. Neurosci. Res.* **2022**, *100*, 1084–1104. [\[CrossRef\]](#)
57. Shahpasand, K. Conformation-Independent Antibodies against Neurotoxic tau Proteins. U.S. Patent No. 10,570,195, 25 February 2020.
58. Han, E.; Li, X.; Zhang, Y.; Zhang, M.; Cai, J.; Zhang, X. Electrochemical immunosensor based on self-assembled gold nanorods for label-free and sensitive determination of *Staphylococcus aureus*. *Anal. Biochem.* **2020**, *611*, 113982. [\[CrossRef\]](#)
59. Badea, M.; Floroian, L.; Restani, P.; Moga, M. Simple surface functionalization strategy for immunosensing detection of aflatoxin B1. *Int. J. Electrochem. Sci.* **2016**, *11*, 6719–6734. [\[CrossRef\]](#)
60. Beseler, C.; Vollmer, T.; Graner, M.; Yu, X. The complex relationship between oligoclonal bands, lymphocytes in the cerebrospinal fluid, and immunoglobulin G antibodies in multiple sclerosis: Indication of serum contribution. *PLoS ONE* **2017**, *12*, e0186842. [\[CrossRef\]](#)
61. Orlovska-Waast, S.; Köhler-Forsberg, O.; Brix, S.W.; Nordentoft, M.; Kondziella, D.; Krogh, J.; Benros, M.E. Cerebrospinal fluid markers of inflammation and infections in schizophrenia and affective disorders: A systematic review and meta-analysis. *Mol. Psychiatry* **2019**, *24*, 869–887. [\[CrossRef\]](#)
62. Kowarik, M.C.; Dzieciatkowska, M.; Wemlinger, S.; Ritchie, A.M.; Hemmer, B.; Owens, G.P.; Bennett, J.L. The cerebrospinal fluid immunoglobulin transcriptome and proteome in neuromyelitis optica reveals central nervous system-specific B cell populations. *J. Neuroinflamm.* **2015**, *12*, 19. [\[CrossRef\]](#) [\[PubMed\]](#)
63. Shao, Y.; Fu, R.; Liu, H.; Wang, Y.; Ding, S.; Wang, H.; Li, L.; Shao, Z. IgG autoantibody subclasses altered in immuno-related hemocytopenia. *Cell Immunol.* **2015**, *294*, 13–20. [\[CrossRef\]](#) [\[PubMed\]](#)
64. Ang, S.H.; Thevarajah, M.; Alias, Y.; Khor, S.M. Current aspects in hemoglobin A1c detection: A review. *Clin. Chim. Acta* **2015**, *439*, 202–211. [\[CrossRef\]](#) [\[PubMed\]](#)
65. Tuantranont, A. Applications of nanomaterials in sensors and diagnostics. In *Springer Series on Chemical Sensors and Biosensors*; Springer: Berlin, Germany, 2013.
66. Derkus, B.; Bozkurt, P.A.; Tulu, M.; Emregul, K.C.; Yucesan, C.; Emregul, E. Simultaneous quantification of Myelin Basic Protein and Tau proteins in cerebrospinal fluid and serum of Multiple Sclerosis patients using nanoimmunosensor. *Biosens. Bioelectron.* **2017**, *89*, 781–788. [\[CrossRef\]](#)
67. Alonso-Lomillo, M.A.; Domínguez-Renedo, O.; Ferreira-Gonçalves, L.; Arcos-Martínez, M.J. Sensitive enzyme-biosensor based on screen-printed electrodes for Ochratoxin A. *Biosens. Bioelectron.* **2010**, *25*, 1333–1337. [\[CrossRef\]](#)
68. Wu, H.; Wang, X.; Qiao, M.; Zhang, H.; Jin, X.; Fan, S. Enhancing sensitivity of hemoglobin-based electrochemical biosensor by using protein conformational intermediate. *Sens. Actuators B Chem.* **2015**, *221*, 694–699. [\[CrossRef\]](#)
69. Hun, X.; Kong, X.J.J.o.P.; Analysis, B. An enzyme linked aptamer photoelectrochemical biosensor for Tau-381 protein using AuNPs/MoSe₂ as sensing material. *J. Pharm. Biomed. Analysis* **2021**, *192*, 113666. [\[CrossRef\]](#)
70. Karaboga, M.N.S.; Sezginürk, M.K.J.T. Analysis of Tau-441 protein in clinical samples using rGO/AuNP nanocomposite-supported disposable impedimetric neuro-biosensing platform: Towards Alzheimer's disease detection. *Talanta* **2020**, *219*, 121257. [\[CrossRef\]](#)
71. Ben Hassine, A.; Raouafi, N.; Moreira, F.T.J.C. Novel electrochemical molecularly imprinted polymer-based biosensor for Tau protein detection. *Chemosensors* **2021**, *9*, 238. [\[CrossRef\]](#)